Available online at www.sciencedirect.com
SCIENCE DIRECT®
Journal of Molecular Spectroscopy 237 (2006) 129–136
Journal of MOLECULAR SPECTROSCOPY
www.elsevier.com/locate/jms

Fourier transform spectroscopy of N_2O weak overtone transitions in the 1–2 μm region

L. Wang [a,b], V.I. Perevalov [b,c], S.A. Tashkun [b,c], B. Gao [a,b], L.-Y. Hao [a], S.-M. Hu [a,b,*]

[a] *Hefei National Laboratory for Physical Sciences at Microscale, Department of Chemical Physics, University of Science and Technology of China, Hefei 230026, China*

[b] *USTC-Shanghai Institute for Advanced Studies, University of Science and Technology of China, Shanghai 201315, China*

[c] *Laboratory of Theoretical Spectroscopy, Institute of Atmospheric Optics SB RAS, 1, Akademicheskii av., 634055 Tomsk, Russia*

Received 24 February 2006; in revised form 10 March 2006
Available online 28 March 2006

Abstract

The absorption spectrum of the natural sample of nitrous oxide has been recorded at Doppler limited resolution with a Fourier-transform spectrometer in the spectral range 5000–10 000 cm^{-1}. Ten cold bands ($8\Sigma - \Sigma$ and $2\Sigma - \Pi$), thirteen hot bands ($11\Pi - \Pi$, $\Sigma - \Sigma$, and $\Delta - \Delta$) of $^{14}N_2{}^{16}O$ and the $3\nu_3$ band of $^{14}N^{15}N^{16}O$ have been newly detected. The uncertainty of the line position determination is estimated to be about 0.005 cm^{-1} for unblended lines. The assignment of the spectrum has been done with the help of the prediction performed within the framework of the polyad model of effective Hamiltonian. The spectroscopic parameters G_v, B_v, D_v, H_v, and q_v have been determined for all newly detected bands. The line intensities of 13 weak bands have been measured. The uncertainty of the obtained line intensity values varies from 7 to 13%.

Keywords: Nitrous oxide; Infrared; Fourier transform spectroscopy; Line positions; Line intensities

1. Introduction

The high-resolution spectra of nitrous oxide are important for several applications. First of all, the nitrous oxide is relatively abundant in the Earth's atmosphere. It gives the non-negligible contribution to the "greenhouse" effect. Then the high-resolution spectra of N_2O together with those of other atmospheric constituents are needed in the processing of the results of the remote-sensing measurements, especially in the cases of the high-resolution satellite-based interferometers. The high-resolution spectra of N_2O can be also used in the monitoring of combustion and some other processes.

The extensive studies of high-resolution spectra of N_2O molecule have been performed by Toth [1–7]. These data were compiled in the linelist SISAM.N_2O [8] the most part of which is incorporated now to the HITRAN2004 database [9]. This list contains the lines with the line intensities larger than 5.0×10^{-6} cm^{-2}/atm at 296 K in the region 525–7796 cm^{-1}. There are many other studies of the high-resolution spectra of nitrous oxide. Here, we mention only those dealing with the spectral region 5000–10 000 cm^{-1} [10–23]. In this paper, we focus on the weak overtone transitions of nitrous oxide in this region. The knowledge of the spectra caused by these transitions gives better understanding of the intramolecular dynamics in this molecule and leads to better global modeling of its high-resolution spectra. This paper is aimed to supply with new data our activity in global modeling of high-resolution spectra of N_2O.

2. Experimental details

The absorption spectra of N_2O were recorded in the spectral range from 5000 to 10 000 cm^{-1} with a Bruker IFS 120HR Fourier-transform spectrometer (FTS)

* Corresponding author. Fax: +86 551 360 2969.
E-mail address: smhu@ustc.edu.cn (S.-M. Hu).

0022-2852/$ - see front matter © 2006 Elsevier Inc. All rights reserved.
doi:10.1016/j.jms.2006.03.007

equipped with a path length adjustable multi-pass gas cell. The maximum optical path length is 105 m. A tungsten source, CaF_2 beam splitter and a Ge diode detector were used in all experiments. The cell was operated at room temperature, stabilized by an air-conditioning system. The abundance of the nitrous dioxide in the sample was 99.7%. The pressure was measured with two capacitance manometers of 200 Pa and 133 hPa full-scale range with an overall accuracy of 0.5%. Different band-pass optic filters were applied to improve the signal to noise ratio. Because of the wide spectral range and the large variation of the absorption line intensities, different experimental conditions were used as listed in Table 1. The line positions were calibrated using the absorption lines of water (present as an impurity in the cell) given in HITRAN [9]. The experimental conditions are presented in Table 1. The accuracy of the unblended lines recorded with a good signal to noise ratio was estimated to be better than 0.005 cm^{-1}. Altogether 9675 scans were co-added to improve the signal-noise-ratio. An overview of the recorded spectrum with a pressure of 200 hPa is presented in Fig. 1.

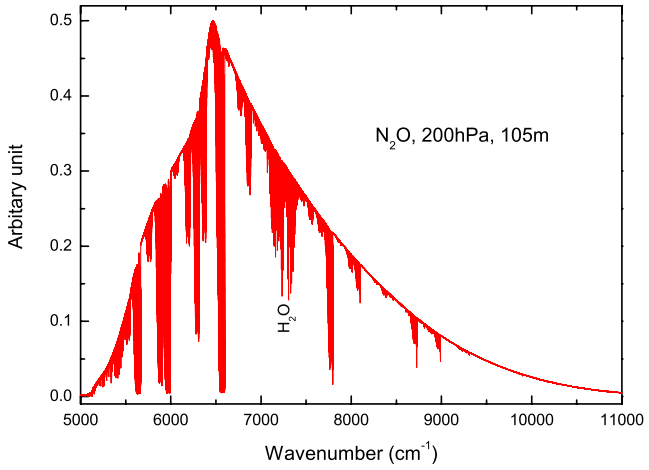

Fig. 1. Overview of the Fourier transform absorption spectrum of N_2O in the region 5000–10000 cm^{-1}.

3. Rovibrational analysis

3.1. Vibrational assignment

The observed transitions have been assigned using the predictions performed with the help of the effective Hamiltonian suggested by Pliva [24] and developed by Teffo et al. [25,26] which is based on a polyad structure of the vibrational states resulting from the approximate relations between the harmonic frequencies $\omega_3 \approx 2\omega_1 \approx 4\omega_2$. The vibrational energy levels are uniquely labeled using the triplet $(P = 2V_1 + V_2 + 4V_3,\ \ell_2,\ i)$, where V_k $(k = 1,2,3)$ are vibrational quantum numbers, ℓ_2 is vibrational angular momentum quantum number, and the index i increases with the energy. In following discussions, we will use the notation (P, ℓ_2, i) instead of $(V_1 V_2^{\ell_2} V_3)$ to identify a vibrational state. The set of effective Hamiltonian parameters obtained by Perevalov et al. [27] was used for the prediction. According to the theory of high-resolution spectra of the rigid molecules there exists the conventional relation between parameters of an effective dipole moment operator

$$\frac{\mu^{\Delta\ell_2}_{\Delta V'_1\Delta V'_2\Delta V'_3}}{\mu^{\Delta\ell_2}_{\Delta V_1\Delta V_2\Delta V_3}} \sim \lambda^{\left(\sum_i |\Delta V'_i| - \sum_i |\Delta V_i|\right)},$$

where $\lambda = \sqrt{\frac{2B}{\bar{\omega}}}$ is the smallness parameter. Here, B is rotational constant and $\bar{\omega}$ is the average value of the harmonic frequencies. As it has been discussed in [18] from this relation follows that the line intensities in the case of the series of transition with even ΔP are determined mostly by the effective dipole moment parameters of the type $\mu^{\Delta\ell_2=0}_{\Delta V_1\Delta V_2=0\Delta V_3}$ and in the case of the series of transitions with add ΔP they are determined by those of the type $\mu^{|\Delta\ell_2|=1}_{\Delta V_1\Delta V_2=\pm1\Delta V_3}$. As the result it is possible to classify the basis states of the upper polyad as "bright" or "dark" states.

All newly observed bands are presented in Table 2. Two of the bands presented in this table centered at 7874 and 8948 cm^{-1} were mentioned for the first time by Herzberg and Herzberg [10] and observed with FTS by Weirauch et al. [17]. But in the later case only a few strongest lines in each band have been detected. In Table 2 together with vibrational assignments the predicted [27] and observed values for the vibrational term values G_v and $\Delta B_v = B_v - B_{GS}$ are presented. Here, B_{GS} is the ground state rotational constant. In this table, we give for the upper vibrational state the basis states with modulo of expansion coefficients larger than 0.4. And as in [17–21], we also present in this table the squares of the expansion coefficients of the upper vibrational state relative to the bright basis states appearing in the eigenvector expansion with a fraction larger than 0.01.

All together we have newly assigned 24 bands: eight $\Sigma - \Sigma$ and two $\Sigma - \Pi$ cold bands of $^{14}N_2O$, one cold $3\nu_3$ band of $^{14}N^{15}N^{16}O$, eleven $\Pi - \Pi$, one $\Sigma - \Sigma$, and one $\Delta - \Delta$ hot bands of $^{14}N_2{}^{16}O$. The $\Sigma - \Sigma$ hot band originates from 10^00 vibrational state and $\Delta - \Delta$ hot band orig-

Table 1
Experimental conditions

Spectral region (cm^{-1})	Pressure (hPa)	Path length (m)	Temperature (K)	Resolution (cm^{-1})	Detector
5000–10000	200.0	105	293.2	0.03	Ge
—	178.2	87	292.6	0.02	Ge
—	151.5	87	291.8	0.02	Ge
—	131.8	87	293.2	0.02	Ge
—	118.1	87	293.4	0.02	Ge

Table 2
Vibrational levels and fractions relative to the bright states

(P,ℓ_2,i)[a]	G_v (cm^{-1})		$\Delta B_v \times 10^2$ (cm^{-1})[b]		Basis states[c] $(v_1, v_2^{\ell_2}, v_3)$	Bright state $(v_1, v_2^{\ell_2}, v_3)$	% Fraction[d]
	Obs.	Calc.	Obs.	Calc.			
$^{14}N_2{}^{16}O$ Cold bands[1)]							
9 1 5[e]	5319.593	5319.588	−0.556	−0.553	$2\ 1^1\ 1/1\ 3^1\ 1$	$2\ 1^1\ 1$	59.3
10 0 9	6058.670	6058.668	−0.172	−0.171	$4\ 2^0\ 0/0\ 10^0\ 0$	$5\ 0^0\ 0$	4.6
11 1 3	6214.228	6214.228	−0.794	−0.795	$1\ 1^1\ 2/0\ 3^1\ 2$	$1\ 1^1\ 2/3\ 1^1\ 1$	79.7/1.3
12 0 7[g]	6882.712	6882.684	−0.303	−0.296	$0\ 8^0\ 1/2\ 4^0\ 1/3\ 2^0\ 1$	$4\ 0^0\ 1$	1.7
12 0 13	7340.794	7340.791	−0.375	−0.373	$5\ 2^0\ 0/0\ 12^0\ 0/3\ 6^0\ 0$	$6\ 0^0 0$	9.9
14 0 5	7874.156	7874.169	−0.686	−0.684	$2\ 2^0\ 2/0\ 6^0\ 2$	$3\ 0^0\ 2$	5.8
14 0 10[g]	8145.544	8145.581	−0.426	−0.437	$4\ 2^0\ 1/0\ 10^0\ 1$	$5\ 0^0\ 1$	4.1
14 0 18[g]	8725.093	8725.137	−0.851	−0.850	$7\ 0^0\ 0$	$5\ 0^0\ 1/7\ 0^0\ 0$	1.7/44.0
14 0 19[g]	8810.780	8810.810	−0.970	−0.952	$7\ 0^0\ 0/6\ 2^0\ 0$	$5\ 0^0\ 1/7\ 0^0\ 0$	1.8/27.7
16 0 2[g]	8739.306	8739.275	−0.833	−0.830	$0\ 4^0\ 3/1\ 2^0\ 3$	$2\ 0^0\ 3$	1.8
Hot bands (*transitions from the first polyad*)[2)]							
11 1 1	6083.729	6083.726	−0.535	−0.536	$0\ 3^1\ 2/1\ 1^1\ 2$	$1\ 1^1\ 2$	18.1
11 1 5	6326.676	6326.675	−0.318	−0.318	$2\ 3^1\ 1/0\ 7^1\ 1$	$3\ 1^1\ 1$	12.2
11 1 9	6631.011	6631.015	−0.145	−0.148	$4\ 3^1\ 0/0\ 11^1\ 0/2\ 7^1\ 0$	$5\ 1^1\ 0$	10.2
11 1 10	6772.934	6772.925	−0.371	−0.372	$5\ 1^1\ 0/0\ 11^1\ 0/\ 1\ 9^1\ 0/3\ 5^1\ 0$	$5\ 1^1\ 0$	32.8
11 1 11[g]	6892.631	6892.627	−0.565	−0.565	$5\ 1^1\ 0/1\ 9^1\ 0/2\ 7^1\ 0$	$5\ 1^1\ 0/3\ 1^1\ 1$	41.7/1.3
11 1 12	6996.429	6996.425	−0.609	−0.610	$3\ 5^1\ 0/4\ 3^1\ 0/2\ 7^1\ 0$	$5\ 1^1\ 0$	11.6
13 1 8[f]	7589.841	7589.830	−0.473	−0.472	$0\ 9^1\ 1/3\ 3^1\ 1/4\ 1^1\ 1$	$4\ 1^1\ 1$	20.3
15 1 8[f]	8559.593	8559.644	−0.891	−0.891	$3\ 1^1\ 2/1\ 5^1\ 2$	$3\ 1^1\ 2/5\ 1^1\ 1/1\ 1^1\ 3$	42.4/2.5/1.0
15 1 9	8666.572	8666.620	−1.083	−1.082	$3\ 1^1\ 2/2\ 3^1\ 2/1\ 5^1\ 2$	$3\ 1^1\ 2/1\ 1^1\ 3\ /5\ 1^1\ 1$	36.1/2.5/1.5
17 1 4[g]	9421.050	9421.209	−1.015	−1.050	$2\ 1^1\ 3/0\ 5^1\ 3/1\ 3^1\ 3$	$2\ 1^1\ 3/4\ 1^1\ 2$	32.6/2.1
17 1 7[g]	9537.661	9537.741	−1.288	−1.293	$2\ 1^1\ 3/1\ 3^1\ 3$	$2\ 1^1\ 3/4\ 1^1\ 2/0\ 1^1\ 4$	55.7/2.9/1.8
Hot bands (*transitions from the second polyad*)							
12 0 6[1)]	6868.548	6868.550	−1.038	−1.039	$2\ 0^0\ 2/1\ 2^0\ 2$	$2\ 0^0\ 2/4\ 0^0\ 1/0\ 0^0\ 3$	70.7/2.5/1.2
16 2 7[3)]	8890.141	8890.212	−1.057	−1.064	$1\ 2^2\ 3$	$1\ 2^2\ 3/3\ 2^2\ 2$	73.3/1.8
$^{14}N^{15}N^{16}O$							
12 0 1[1)]	6446.894	6446.894	−0.999	−1.001	$0\ 0^0\ 3$	$0\ 0^0\ 3$	92.5

[a] Cluster labelling notation: $(P = 2V_1 + V_2 + 4V_3, \ell_2, i)$; i is the order number within the cluster increasing with the energy.
[b] $\Delta B_V = B_V - B_{GS}$, ground state constants B_{GS} are taken from [28] for $^{14}N_2{}^{16}O$ and from [8] for $^{14}N^{15}N^{16}O$.
[c] Only basis states with modulo of expansion coefficients larger than 0.4 are presented.
[d] Square of the expansion coefficient of the vibrational state relative to the bright basis states appearing in the eigenvector expansion with a fraction larger than 0.01: [1)] relative to $(V_1, V_2^{\ell_2} = 0^0, V_3)$, [2)] relative to $(V_1, V_2^{\ell_2} = 1^1, V_3)$, [3)] relative to $(V_1, V_2^{\ell_2} = 2^2, V_3)$.
[e] Constants are given for f sublevel because only Q branch ($f \leftarrow e$) of the (9 1 5) – (0 0 1) band was observed.
[f] Perturbed band (intrapolyad resonance interaction).
[g] Perturbed band (interpolyad resonance interaction).

inates from 02^20 vibrational state. Though two bands centered at 7874 and 8948 cm^{-1} have been observed earlier they were analyzed for the first time. As an example, in Fig. 2 the Q branch of the perpendicular cold band (9 1 5) – (0 0 1) centered at 5319.592 cm^{-1} is presented. Another example is given in Fig. 3 where the P branch of $3\nu_3$ band of $^{14}N^{15}N^{16}O$ together with R branch of the parallel hot band (11 1 12) – (1 1 1) are presented.

As one can see from Table 2, in the majority of the cases there is good agreement between predicted and observed values of the vibrational energy and rotational constants. Some cases where the significant disagreement is observed will be discussed below.

3.2. Band by band rotational analysis

The band by band rotational analysis was performed using the standard expression for the rotational energy levels in a given vibrational state:

$$E_v(J,\ell_2) = G_v + B_v[J(J+1) - \ell_2^2] - D_v[J(J+1) - \ell_2^2]^2 + H_v[J(J+1) - \ell_2^2]^3 \pm \tfrac{1}{2} q_v J(J+1), \quad (1)$$

where (+) is used for the f sublevel and (−) for the e sublevel of the vibrational state with $\ell_2 \neq 0$. Here, G_v is the vibrational term value, B_v is the rotational constant, D_v and H_v are centrifugal distortion constants, and q_v is the ℓ—doubling constant. These constants for an upper state have been fitted to the observed line positions of the respective observed band. The lower state constants have been fixed to the literature values: the ground state constants and constants for the 01^10 and 10^00 vibrational states of $^{14}N_2{}^{16}O$ were taken from [28], the constants for the 02^20 vibrational state of $^{14}N_2{}^{16}O$ and ground state constants of $^{14}N^{15}N^{16}O$ were taken from [8]. In [28,8] the expressions for the vibration-rotation energies differ from Eq. (1) in this work. Therefore, the spectroscopic constants from [28,8] were recalculated to those definition according to Eq. (1). In Table 3, we present the fit-

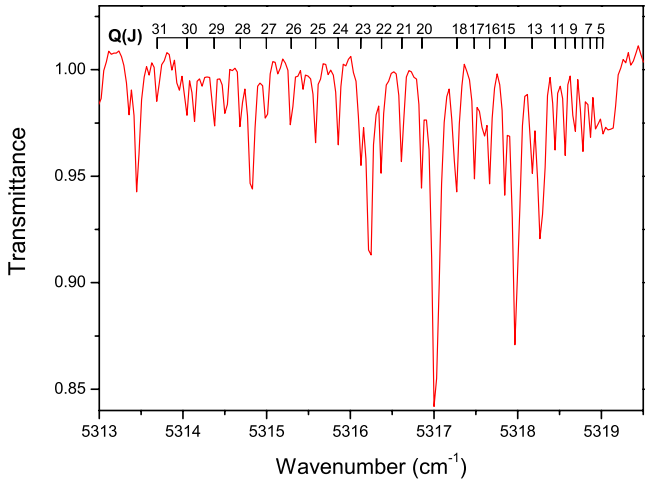

Fig. 2. The Q branch of the perpendicular cold band $(915)-(001)$ centered at 5319.592 cm^{-1}.

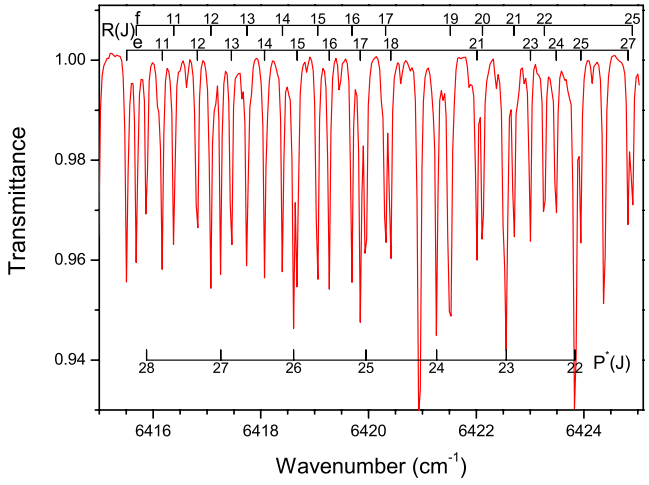

Fig. 3. The P branch of $3\nu_3$ band of $^{14}N^{15}N^{16}O$ centered at 6446.894 cm^{-1} and R branch of parallel hot band $(11112)-(111)$ of $^{14}N_2{}^{16}O$ centered at 6407.248 cm^{-1}.

ted values of the spectroscopic constant for all observed bands. It is necessary to emphasize that the spectroscopic constants for the $(11111)-(111)$ band are meaningless for low J values because this band is strongly perturbed by $(12212)-(111)$ band at low J values. All measured wavenumbers and rotational assignments are available in Supplementary Materials (I).

4. Vibration–rotation perturbations

Our theoretical consideration shows that even below $J=60$ the majority of the observed bands are perturbed. In Table 2 the perturbed bands are marked by symbol "f" in the case of intrapolyad resonance interactions and by symbol "g" in the case of interpolyad resonance interactions. The most pronounced perturbations are due to the energy level crossings. The respective perturbed bands are listed in Table 4. In this table the types of the resonance interactions and the values of the angular momentum quantum number J at which the crossing takes place are given.

In most cases the evidence of the perturbations was not demonstrated by the fitting of the spectroscopic constants to the observed line positions. There are two reasons for this: the observed line positions lie rather far from the energy level crossings and the limited accuracy of the line position determination does not allow detecting the perturbations. Only in two cases the perturbations were observed. The most pronounced of them is the case of $(11111)-(111)$ band which is perturbed by $(12212)-(111)$ band via interpolyad resonance Coriolis interaction. The respective matrix element of effective Hamiltonian is

$$\left\langle V_1+1(V_2+1)^{\ell_2\pm1}V_3-1\ J\ K\pm1\middle|H^{\mathrm{eff}}\middle|V_1V_2^{\ell_2}V_3JK\right\rangle. \quad (2)$$

In Fig. 4 the unperturbed energy differences between (11111) and (12212) upper vibrational states versus angular momentum quantum number J are plotted. This figure clearly shows the energy level crossings at $J=10$ (e sublevel) and at $J=15$ (f sublevel). This very strong perturbation leads to the difference between observed and calculated with the help of spectroscopic parameters line position of the line $P_f(18)$ equal to 0.157 cm^{-1} (see Fig. 5). Small perturbations of the $R(10)-R(15)$ lines of the $(12007)-(00001)$ band were also observed. For this band only R branch was detected. We identify this perturbation as a result of Coriolis interactions between three vibrational states (11111), (12212), and (12007).

In the result of our theoretical analysis it was found several additional cases of interpolyad resonance interactions in the case of newly observed bands. The interpolyad resonance Coriolis interaction due to the matrix element (2) takes place for the $(14010)\leftrightarrow(13115)$ and $(14018)\leftrightarrow(15110)$ pairs of the vibrational states. The resonance anharmonic interaction takes place for the $(14018)\leftrightarrow(16002)$, $(14019)\leftrightarrow(16003)$, $(17114)\leftrightarrow(15119)$, and $(17117)\leftrightarrow(15120)$ pairs of vibrational states. The following matrix element of the effective Hamiltonian

$$\left\langle V_1+3\ V_2\ V_3-2\ J\middle|H^{\mathrm{eff}}\middle|V_1V_2^{\ell_2}V_3JK\right\rangle \quad (3)$$

is responsible for these interactions.

In our opinion the above discussed interpolyad resonance interactions which are not taken into account by polyad model of effective Hamiltonian explain rather large residuals between our predicted and measured line positions for some of the observed bands.

5. Retrieval of the line strengths data

A PC based program "Intwin" written in C++ was applied to obtain the line parameters from the profile fitting to the observed spectrum. For the study of the line intensities, to speed up the line profile fitting procedure,

Table 3
Spectroscopic constants (in cm^{-1}) for the newly observed bands of N_2O in the region 5200–9000 cm^{-1}

Band[a]	Type	v_0[b]	G_v	B_v	$D_v \times 10^7$	$H_v \times 10^{10}$	$q_v \times 10^3$	J_{max}[c] $P/Q/R$	n/N[d]	Rms $\times 10^3$[e]
Spectroscopic constants for the cold bands of $^{14}N_2{}^{16}O$										
(9 1 5) – (0 0 1)[f]	Π – Σ	5319.1794(16)	5319.5928(16)	0.4134450(92)	1.285(99)			/30/	21/24	3.12
(10 0 9) – (0 0 1)	Σ – Σ	6058.67008(80)	6058.67008(80)	0.4172870(34)	5.129(27)			37/ /36	71/86	3.37
(11 1 3) – (0 0 1)	Π – Σ	6213.8169(11)	6214.2280(11)	0.4110766(49)	1.916(41)		0.8706(15)	28/34/33	47/58	3.06
(12 0 7) – (0 0 1)	Σ – Σ	6882.7117(16)	6882.7117(16)	0.4159792(49)	4.985(28)			/ /40	25/34	3.24
(12 0 13) – (0 0 1)	Σ – Σ	7340.7938(15)	7340.7938(15)	0.4152602(72)	5.003(68)			28/ /31	29/34	2.89
(14 0 5) – (0 0 1)	Σ – Σ	7874.15620(62)	7874.15620(62)	0.4121491(28)	3.474(22)			37/ /35	68/84	2.63
(14 0 10) – (0 0 1)	Σ – Σ	8145.5436(20)	8145.5436(20)	0.414764(27)	15.05(84)	6.24(73)		27/ /26	31/50	3.05
(14 0 18) – (0 0 1)	Σ – Σ	8725.0932(13)	8725.0932(13)	0.4105047(70)	2.822(71)			23/ /30	23/36	2.84
(16 0 2) – (0 0 1)	Σ – Σ	8739.3055(19)	8739.3055(19)	0.410676(18)	3.55(32)			13/ /22	21/37	3.29
(14 0 19) – (0 0 1)	Σ – Σ	8810.7796(18)	8810.7796(18)	0.409334(16)	−3.47(27)			24/ /18	26/33	3.01
Spectroscopic constants for the $3v_3$ band of $^{14}N^{15}N^{16}O$										
(12 0 1) – (0 0 1)	Σ – Σ	6446.89423(78)	6446.89423(78)	0.4089692(36)	1.730(31)			37/ /30	62/69	3.08
Band[a]	Type	v_0	ΔG_v	G_v	B_v	$D_v \times 10^7$	$q_v \times 10^3$	J_{max}[g] $P/Q/R$	n/N	Rms $\times 10^3$
Spectroscopic constants for the hot bands of $^{14}N_2{}^{16}O$										
(11 1 1) – (1 1 1)	Π – Π	5494.5475(13)	5494.5416(13)	6083.7289	0.4136587(55)	2.172(46)	1.4374(14)	35/ /33, 32/ /31	65/102	3.28
(12 0 6) – (2 0 2)	Σ – Σ	5583.6442(15)	5583.6442(15)	6868.5475	0.4086321(74)	1.608(79)		27/ /30	31/34	3.17
(11 1 5) – (1 1 1)	Π – Π	5737.4923(10)	5737.4885(10)	6326.6758	0.4158348(41)	2.620(31)	2.2241(11)	36/ /33, 37/ /34	74/117	3.28
(11 1 9) – (1 1 1)	Π – Π	6041.8256(11)	6041.8236(11)	6631.0109	0.4175581(73)	3.604(97)	3.1710(22)	27/ /27, 26/ /26	56/73	3.18
(11 1 10) – (1 1 1)	Π – Π	6183.75073(84)	6183.74646(84)	6772.9338	0.4153015(33)	2.645(23)	2.6171(13)	35/ /29, 41/ /22	63/92	2.95
(11 1 11) – (1 1 1)	Π – Π	6303.4497(16)	6303.4434(16)	6892.6307	0.4133510(34)	1.754(16)	2.1078(1.1)	30/ /46, 34/ /38	45/95	2.90
(11 1 12) – (1 1 1)	Π – Π	6407.24794(63)	6407.24129(63)	6996.4286	0.4129227(24)	1.134(16)	2.0864(22)	28/ /41, 25/ /25	66/103	3.03
(13 1 8) – (1 1 1)	Π – Π	7000.6587(12)	7000.6534(12)	7589.8407	0.4142718(67)	4.617(76)	2.4013(24)	26/ /24, 32/ /28	48/77	3.15
(16 2 7) – (2 2 2)	Δ – Δ	7710.7630 (23)	7710.7163(23)	8890.1414	0.408451 (15)	1.15 (19)		19/ /26	22/33	3.49
(15 1 8) – (1 1 1)	Π – Π	7970.4149(11)	7970.4054(11)	8559.5927	0.4101066(50)	1.760(42)	1.6589(19)	37/ /29, 31/ /25	59/100	3.48
(15 1 9) – (1 1 1)	Π – Π	8077.3962(14)	8077.3848(14)	8666.5721	0.4081720(54)	1.266(41)	1.2459(14)	36/ /15, 36/ /19	46/90	3.09
(17 1 4) – (1 1 1)	Π – Π	8831.8734(34)	8831.8627(34)	9421.0500	0.408911(33)	8.11(72)	1.5223(56)	16/ /19, 19/ /16	24/39	3.33
(17 1 7) – (1 1 1)[h]	Π – Π	8948.4873(12)	8948.4740(12)	9537.6613	0.406232(17)	5.25(39)		22/ /8	23/24	3.04

[a] The lower vibrational states (001), (111), (202) and (222) correspond respectively to $0\ 0^0\ 0$, $0\ 1^1\ 0$, $1\ 0^0\ 0$, and $0\ 2^2\ 0$ states in the harmonic oscillator quantum numbers notations.
[b] v_0 is the band center.
[c] J_{max} is the maximum value of the angular momentum quantum number observed for $P/Q/R$ branches.
[d] n is the number of fitted line positions and N is the total number of assigned lines.
[e] Rms is the root mean squares of the residuals.
[f] Constants are given for f sublevel because only Q branch ($f \leftarrow e$) of the (915) – (001) band was observed.
[g] Upper line for e–e transitions and lower line for f–f transitions.
[h] Constants are given for e sublevel because only $e \leftarrow e$ sub band of the (1717) – (111) band was observed.

Table 4
Predicted local ro-vibrational perturbations in the observed bands of N_2O

State	Perturber	J_{pert}[a]	Interaction type
(12 0 7)	(11 1 11)	58	Coriolis
(14 0 19)	(16 0 3)	26	Anharmonic
(11 1 11)	(12 2 12)	*e*: 10; *f*: 15	Coriolis
(15 1 8)	(15 1 7)	*e*: 46; *f*: 40	Anharmonic
(17 1 4)	(15 1 19)	1	Anharmonic
(17 1 7)	(15 1 20)	*e*: 30; *f*: 25	Anharmonic

[a] Value of the angular momentum quantum number at which the energy level crossing takes place.

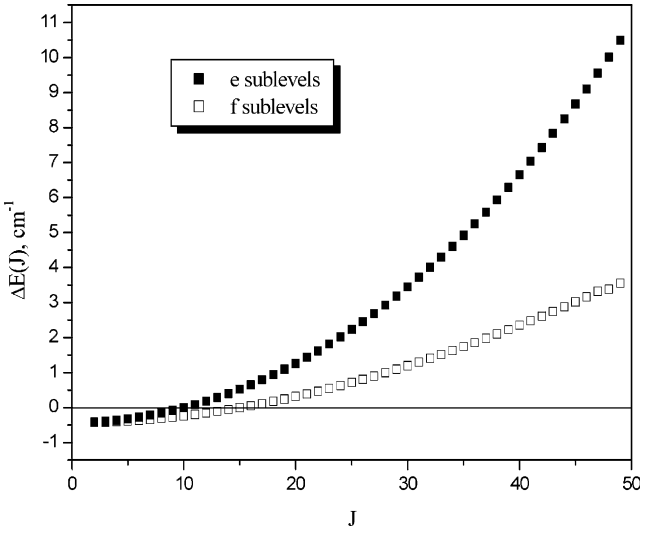

Fig. 4. The unperturbed energy differences between (11111) and (12212) vibrational states versus angular momentum quantum number *J*.

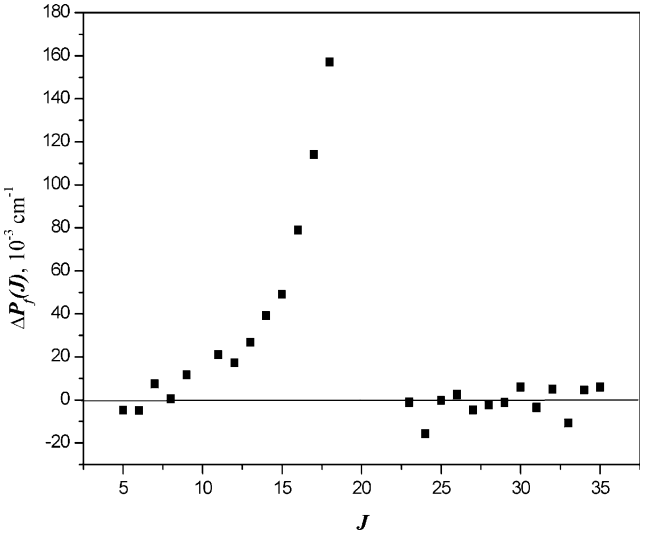

Fig. 5. The residuals between observed and calculated (with the help of spectroscopic constants) values of the line positions for the P_f—branch of the (11111) – (111) hot band of $^{14}N_2{}^{16}O$ centered at 6303.450 cm^{-1}.

the Blackman–Harris 3 term (BH3T)[1] apodization function was used. Voigt profile was adopted for each line. The fitting spectral region is determined as several times of the line widths. If several lines are overlapped or very close to each other, the fitting region will be automatically enlarged to include all these lines. The Levenberg–Marquardt algorithm was used in the least square fitting procedure to minimize the deviation between the observed and calculated spectrum. Line position, integrated line absorbance, Gaussian and Lorentzian widths of each line and a baseline (as a linear function of the wavenumber) can be obtained from the fitting procedure. The Gaussian widths can be fixed at the corresponding Doppler width.

In our measurements, the pressure uncertainty is about 1% and the error from the temperature fluctuation and absorption path length is about 0.5%. For the weak bands, which are studied in this paper, the fitting error is estimated to be around 5% for well-isolated lines. Including all errors mentioned above, we estimated the accuracy of our line intensities to be 7% or better for the majority of the lines and about 13% for very weak lines.

The absolute line intensities or integrated absorption coefficients per unit pressure $\tilde{S}(T)$, in cm^{-2} atm^{-1} at temperature T, were deduced from the integrated line absorbance I using the equation

$$\tilde{S}(T) = I/PL, \tag{4}$$

where P is the partial pressure of the studied isotopic species and L is the absorption path length. Then each $\tilde{S}(T)$ value was converted into the absorption line strength, $S(T_0)$, in $cm^{-1}/(molec\ cm^{-2})$ at the standard temperature $T_0 = 296$ K, according to the following equation

$$S(T_0) = \frac{T}{273.15}\frac{1}{N}\frac{Q(T)}{Q(T_0)}\exp\left[\frac{hc}{k}E''\left(\frac{1}{T}-\frac{1}{T_0}\right)\right]\tilde{S}(T), \tag{5}$$

where $N = 2.68676\times10^{19}$ molec cm^{-3} atm^{-1} is Loschmidt's number, h is Plank's constant, c is the speed of light in vacuum, k is Boltzmann's constant, E'' (in cm^{-1}) is the energy of the lower ro-vibrational level of the transition, and Q is the total internal partition function which can be calculated using Eq. (5) from [29]. The summery of the line intensities retrieval is presented in Table 5. The $S(T_0)$ values are given in the Supplementary Material (II).

The line intensities of four bands centered at 6768.50, 6868.55, 7137.13, and 7214.68 cm^{-1} have also been measured before by Toth [6]. Daumont et al. [23] have measured the line intensities of ten from the thirteen measured in this paper bands. In Fig. 6, we give the comparison of our measured line strengths to those of Toth [6] and Daumont et al. [23] for three bands centered at 6868.55, 7137.13, and 7214.68 cm^{-1}. These bands are contained in the linelist SISAM.N2O [8]. As one can see from this figure that our line strengths are in average

[1] BH3T (Blackman–Harris 3 term) function: $W(\Delta) = a_0 + a_1\cos(2\pi\ \Delta/\Delta_m) + a_2\ \cos(4\pi\Delta/\Delta_m)$, where $a_0 = 0.42323$, $a_1 = 0.49755$, $a_2 = 0.07922$, and Δ_m is the maximum optical path difference.

Table 5
Summary of the line intensities retrieval

Band	Band centre (cm^{-1})	J_{max}	Number of lines
(12 0 4) – (0 0 1)	6768.50	43	77
(12 0 6) – (0 0 1)	6868.55	46	77
(12 0 8) – (0 0 1)	7024.09	34	64
(12 0 10) – (0 0 1)	7137.13	48	64
(12 0 12) – (0 0 1)	7214.68	40	68
(12 0 14) – (0 0 1)	7463.99	39	73
(12 0 15) – (0 0 1)	7556.14	40	73
(14 0 1) – (0 0 1)	7665.28	36	62
(14 0 8) – (0 0 1)	7998.59	37	71
(14 0 9) – (0 0 1)	8083.96	46	73
(14 0 14) – (0 0 1)	8376.35	30	53
(16 0 1) – (0 0 1)	8714.14	42	64
(16 0 7) – (0 0 1)	8976.49	40	61

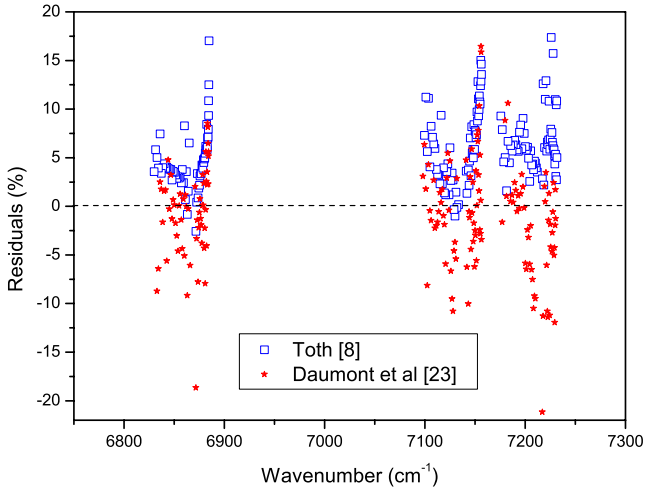

Fig. 6. The residuals $(S_{our} - S_{Toth})/S_{our}$ and $(S_{our} - S_{Daumont})/S_{our}$ in percent between our measured line intensities, S_{our}, and those of Toth [8], S_{Toth}, and of Daumont et al. [23], $S_{Daumont}$, for the bands centered at 6868.55, 7137.13, and 7214.68 cm^{-1}.

5–7% higher than those of Toth [8] and they are in a rather good agreement with the values of Daumont et al. [23]. The large residuals for some weak lines are due to the experimental uncertainties which may reach 20% or even higher in all these measurements. In Fig. 7 the comparison of our measured line strengths with those of Daumont et al. [23] is given for seven bands centered at 7024.09, 7463.99, 7556.14, 7665.28, 7998.59, 8083.96, and 8376.35 cm^{-1}. As shown on this figure our line strengths for these bands are in average 5% lower than those of Daumont et al. [23].

6. Conclusion

New experimental information about twenty three week bands of $^{14}N_2{}^{16}O$ and the $3\nu_3$ band of $^{14}N^{15}N^{16}O$ lying in the region 5000–9500 cm^{-1} has been obtained with a Bruker IFS 120 HR Fourier-transform spectrometer. The half of these bands is found to be involved into interpolyad resonance interactions. The obtained experimental

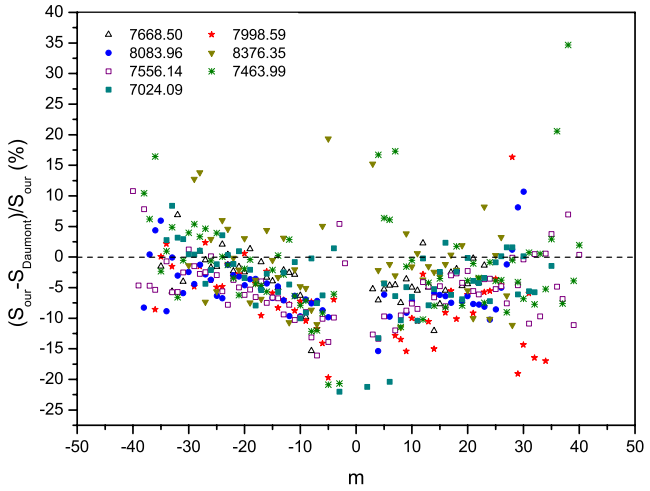

Fig. 7. The residuals $(S_{our} - S_{Daumonl})/S_{our}$ in percent between our measured line intensities, S_{our}, and those measured by Daumont et al. [23], $S_{Daumont}$, for the bands centered at 7024.09, 7463.99, 7556.14, 7665.28, 7998.59, 8083.96, and 8376.35 cm^{-1}. Here, $m = -J$ for P branch and $m = J + 1$ for R branch.

information is very important for our activity in global modeling of high-resolution spectra of N_2O molecule. It has been shown once again (see also [17–21]) that a polyad model of effective Hamiltonian gives the possibility to understand the N_2O high-resolution spectrum and to perform its unambiguous assignment, but to perform the predictions of the line positions with near experimental accuracy it is necessary to use the non-polyad model which takes into account interpolyad resonance interactions in the effective Hamiltonian. The line intensities of 13 weak bands lying in the range from 6700 to 9000 cm^{-1} have been measured. The obtained information is very important for the modeling of the line intensities of N_2O molecule in the high frequency region.

Acknowledgments

This work was jointly supported by the National Project for the Development of Key Fundamental Sciences in China, the Natural Science Foundation of China (20473079, 10274077), by the Chinese Academy of Science, by the Russian Academy of Sciences within the framework of the program No. 2.10 "Optical Spectroscopy and Frequency Standards" and by Siberian Branch of Russian Academy of Sciences within the framework of the integration project No. 187 "Internet Accessible Information System "Spectral Properties of Hot Combustion Gases." VIP and SAT acknowledge the financial support from the Foundation for Educational Development and Research of USTC-SIAS.

Appendix A. Supplementary data

Supplementary data for this article are available on ScienceDirect (www.sciencedirect.com) and as part of the Ohio State University Molecular Spectroscopy Archives (http://msa.lib.ohio-state.edu/jmsa_hp.htm).

References

[1] R.A. Toth, Appl. Opt. 23 (1984) 1825–1834.
[2] R.A. Toth, J. Opt. Soc. Am. B 3 (1986) 1263–1281.
[3] R.A. Toth, J. Opt. Soc. Am. B 4 (1987) 357–374.
[4] R.A. Toth, Appl. Opt. 30 (1991) 5289–5315.
[5] R.A. Toth, Appl. Opt. 32 (1993) 7326–7365.
[6] R.A. Toth, J. Mol. Spectrosc. 197 (1999) 158–187.
[7] R.A. Toth, J. Quant. Spectrosc. Radiat. Transfer 66 (2000) 285–304.
[8] R.A. Toth, available from: <http://mark4sun.jpl.nasa.gov/data/>.
[9] L.S. Rothman, D. Jacquemart, A. Barbe, D.C. Benner, M. Birk, L.R. Brown, M.R. Carleer, C. Chakerian Jr., K.V. Chance, V. Dana, V.M. Devi, J.-M. Flaud, R.R. Gamache, A. Goldman, J.-M. Hartmann, K.W. Jucks, A. Maki, J.-Y. Mandin, S.T. Massie, J. Orphal, A. Perrin, C.P. Rinsland, M.A.H. Smith, J. Tennysson, R.N. Tolchenov, R.A. Toth, J. Vander Auwera, P. Varanasi, G. Wagner, J. Quant. Spectrosc. Radiat. Transfer 96 (2005) 139–204.
[10] G. Herzberg, L. Herzberg, J. Chem. Phys. 18 (1950) 1551–1561.
[11] C. Amiot, G. Guelachvili, J. Mol. Spectrosc. 51 (1974) 475–491.
[12] G.A. Vandysheva, L.N. Sinitsa, Atmos. Opt. 2 (1992) 721–723.
[13] A. Campargue, D. Permogorov, M. Bach, M. Abbouti Temsamani, J. Vander Auwera, M. Herman, M. Fujii, J. Chem. Phys. 103 (1995) 5931–5938.
[14] Y. He, M. Hippler, M. Quack, J. Chem. Phys. Lett. 289 (1998) 527–534.
[15] M. Hippler, M. Quack, J. Chem. Phys. Lett. 314 (1999) 273–281.
[16] H. Oshika, A. Toba, M. Fujitake, N. Ohashi, J. Mol. Spectrosc. 197 (1999) 324–325.
[17] G. Weirauch, A.A. Kachanov, A. Campargue, M. Bach, M. Herman, J. Vander Auwera, J. Mol. Spectrosc. 202 (2000) 98–106.
[18] A. Campargue, G. Weirauch, S.A. Tashkun, V.I. Perevalov, J.-L. Teffo, J. Mol. Spectrosc. 209 (2001) 198–206.
[19] E. Bertseva, A.A. Kachanov, A. Campargue, Chem. Phys. Lett. 351 (2002) 18–26.
[20] Y. Ding, V.I. Perevalov, S.A. Tashkun, J.-L. Teffo, S. Hu, E. Bertseva, A. Campargue, J. Mol. Spectrosc. 220 (2003) 80–86.
[21] E. Bertseva, A. Campargue, V.I. Perevalov, S.A. Tashkun, J. Mol. Spectrosc. 226 (2004) 196–200.
[22] L. Daumont, J. Vander Auwera, J.-L. Teffo, V.I. Perevalov, S.A. Tashkun, J. Mol. Spectrosc. 208 (2001) 281–291.
[23] L. Daumont, J. Vander Auwera, J.-L. Teffo, V.I. Perevalov, S.A. Tashkun, in preparation.
[24] J. Pliva, J. Mol. Spectrosc. 27 (1968) 461–488.
[25] J.-L. Teffo, A. Chedin, J. Mol. Spectrosc. 135 (1989) 389–409.
[26] J.-L. Teffo, V.I. Perevalov, O.M. Lyulin, J. Mol. Spectrosc. 168 (1994) 390–403.
[27] V. I. Perevalov, S.A. Tashkun, J.-L. Teffo, submitted for publication.
[28] M.D. Vanek, M. Schneider, J.S. Wells, A.G. Maki, J. Mol. Spectrosc. 134 (1989) 154–158.
[29] R.R. Gamache, R.L. Hawkins, L.S. Rothman, J. Mol. Spectrosc. 142 (1990) 205–219.